JPE 18-4-7

https://doi.org/10.6113/JPE.2018.18.4.1015
ISSN(Print): 1598-2092 / ISSN(Online): 2093-4718

Family of Dual-Input Dual-Buck Inverters Based on Dual-Input Switching Cells

Fan Yang*, Hongjuan Ge*,**, Jingfan Yang*, Runyun Dang*, and Hongfei Wu†

†,*College of Automation Engineering, Nanjing University of Aeronautics and Astronautics, Nanjing, China
**College of Civil Aviation, Nanjing University of Aeronautics and Astronautics, Nanjing, China

Abstract

A family of dual-DC-input (DI) dual-buck inverters (DBIs) is proposed by employing a DI switching cell as the input of traditional DBIs. Three power ports, i.e. a low voltage DC input port, a high voltage DC input port and an AC output port, are provided by the proposed DI-DBIs. A low voltage DC source, whose voltage is lower than the peak amplitude of the AC side voltage, can be directly connected to the DI-DBI. This supplies power to the AC side in single-stage power conversion. When compared with traditional DBI-based two-stage DC/AC power systems, the conversion stages are reduced, and the power rating and power losses of the front-end Boost converter of the DI-DBI are reduced. In addition, five voltage-levels are generated with the help of the two DC input ports, which is a benefit in terms of reducing the voltage stresses and switching losses of switches. The topology derivation method, operation principles, modulation strategy and characteristics of the proposed inverter are analyzed in-depth. Experimental results are provided to verify the effectiveness and feasibility of the proposed DI-DBIs.

Key words: Circuit topology, Dual-Buck, Dual-input, High efficiency, Inverter

I. INTRODUCTION

Inverters are key elements for the interface an AC load or grid and various DC sources. They have been widely used in renewable energy power systems, micro-grids, uninterruptable power supplies, air-plane power systems and so on [1], [2]. Despite their long history, inverter topologies are still evolving. The search for new inverter topologies with a higher efficiency and a high reliability has never stopped in an effort to meet the requirements of various new applications. As a result, new topological variations and innovations have been continuously emerging [3], [4].

Generally speaking, inverter topologies can be classified into three types: Buck-type, Boost-type and Buck-Boost type. Among them, the buck type inverters, e.g. full-bridge inverters, are more popular due to their simplicity and high efficiency. However, full-bridge inverters, whose switching legs are composed of two active switches in an in-series connection, have the potential for a dangerous short-through [5]. The reverse recovery problem of the body-diodes of active switches is another threat to the reliability and efficiency of full-bridge inverters [6]. The reverse-recovery problem can be avoided by adopting SiC diodes. However, the forward-voltage of a SiC diode is much higher than that of a Si diode or the body-diode of a Si switch. Therefore, it is very difficult to make the current commutate to a SiC diode by paralleling a SiC diode with a Si switch. In addition, the short-through problem cannot be solved when SiC diodes are used in full-bridge inverters. In order to overcome these drawbacks, dual-buck inverters (DBIs) were proposed by splitting the switching-leg in the full-bridge inverter into two buck-type switching-legs [7]-[11]. Since the switching-leg of a DBI is composed of a series-connected active switch and diode. The problems of short-through and reverse-recovery of the body diodes can be solved perfectly. Therefore, DBIs have attracted a lot of attention for use in high reliability and high efficiency applications, such as airplane power systems and the grid-tied inverters for renewable power systems [12]-[14].

Since the DBI is a buck type converter, another Boost converter has to be used as the front-end DC-DC converter if

Manuscript received Feb. 15, 2017; accepted Mar. 1, 2018
Recommended for publication by Associate Editor Sangshin Kwak.
†Corresponding Author: wuhongfei@nuaa.edu.cn
Tel: +86-25-84896005, Fax: +86-25-84896005, Nanjing University of Aeronautics and Astronautics
*College of Automation Engineering, Nanjing University of Aeronautics and Astronautics, China
**College of Civil Aviation, Nanjing University of Aeronautics and Astronautics, China

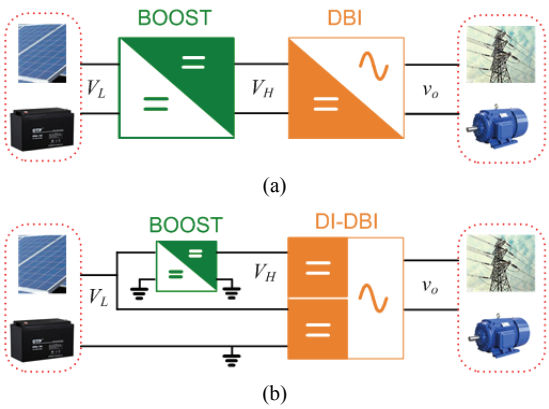

Fig. 1. Two kinds of DC-AC power conversion system: (a) DBI-based; (b) DI-DBI-based.

the voltage of the DC input is lower than the peak amplitude of the AC output voltage. As a result, all of the input power has to be processed by both the front-end Boost converter and the downstream DBI, which hurts the overall efficiency of the DC-AC power system. Although a lot of efforts have been made to improve the efficiency of DBI topologies [15], [16], the power rating and power losses of the front-end Boost converter cannot be reduced. When the DC input voltage is lower than the peak amplitude of the AC output voltage, a Boost type or buck-boost type inverter is more promising in terms of reducing the conversion stages [17]-[20]. However, even though single-stage power conversion can be achieved with a Boost or Buck-Boost type inverter, the conversion efficiency of the Boost or Buck-Boost type inverter is usually lower than that of a buck-type inverter due to the high voltage/current stresses of the devices as well as their complicated topologies and controls.

It is noted that the AC side voltage of an inverter periodically varies between zero and its peak value, which means that the instantaneous value of the AC voltage is not always higher than the voltage of the low voltage DC energy source. This suggests that a low voltage DC input source can directly supply power to an inverter in single-stage power conversion if a low voltage DC input port can be introduced to the inverter. The major contribution of this paper is to propose a new family of dual-DC-input dual-buck inverters (DI-DBIs) to improve the overall conversion efficiency of DC-AC power systems. The structures of the proposed DI-DBI-based and traditional DBI-based DC-AC power conversion systems are shown in Fig. 1. It is important to note that the proposed inverter is referred to as a dual-input dual-buck inverter because both V_L and V_H are DC inputs for the inverter stage. However, in terms of the entire DC-AC power system, the V_H port is an intermediate DC-bus, not a real DC source, and that only the V_L port is a DC source. In practice, like the intermediate DC-bus in a conventional two-stage DC-AC power system, the V_H port for the DI-DBI is provided by a front-end Boost converter. The V_L and V_H ports are the input and output of the Boost converter, respectively. With the proposed DI-DBIs, the power conversion stage is reduced and the efficiency of the DC-AC power system is improved. In addition, the power stress of the front-end Boost is significantly reduced. Therefore, the power losses, power rating and cost of the Boost converter are all reduced as well. Moreover, the multi-level characteristic is realized with the proposed DI-DBIs, which is beneficial for the reduction of switching loss.

II. Derivation of DI-DBI Topologies

The proposed DI-DBI is derived by cascading a dual-input switching cell and a traditional DIB topology. The general structure of the proposed DI-DBI is shown in Fig. 2, where it can be seen that the dual-input switching cell is used as the input of the DBI. Therefore, the dual-input switching cell is the key for the generation of DI-DBI topologies.

Four types of dual-input switching cells are illustrated in Fig. 3. It can be seen that the dual-input switching cell is composed of a high voltage DC source V_H, a low voltage DC source V_L, a active switch S_H and a diode D_L or active switch S_L. The two voltage sources can share a common ground, as shown in Fig. 3(a) and Fig. 3(b), or can be connected in series, as shown in Fig. 3(c) and Fig. 3(d). For the switching cells in Fig. 3(a) and Fig. 3(b), the voltage of V_H must be greater than V_L. Meanwhile, there are no limitations on the voltages of V_H and V_L for the switching cells in Fig. 3(c) and Fig. 3(d). In Fig. 3(a) and Fig. 3(c), the diode D_L is in-series with V_L, which means that V_L can only output power to the downstream DBI. In Fig. 3(b) and Fig. 3(d), an active switch S_L is used to connect V_L. Therefore, the power flows of both V_L and V_H can be bidirectional.

The operation principles of the four dual-input switching cells are all similar. Take the dual-input switching cell in Fig. 3(a) as an example. Since the voltage V_H is greater than V_L, the diode D_L is reverse-biased when S_H is ON. Therefore, once S_H is ON, the high voltage DC source V_H supplies power to the downstream DBI. When S_H is OFF, D_L conducts so that V_L supplies power to the inverter. Obviously, by regulating the ON/OFF states of S_H and D_L, the two DC inputs can alternatively supply power to the inverter.

The topologies of the proposed DI-DBI can be derived by cascading the dual-input switching cell in Fig. 3 and a traditional single-input DBI. Following this principle, a family of DI-DBI topologies, which can simultaneously interface a low voltage DC source and a high voltage DC source, can be derived. Three examples of the proposed DI-DBIs are shown in Fig. 4. These topologies are obtained based on the dual-input switching cell shown in Fig. 3(a). The three single-input DBIs used in Fig. 4(a), Fig. 4(b) and Fig. 4(c) can be found in [7], [8] and [9], respectively. It should be noted that the DI-DBIs are not limited to the ones shown in Fig. 4. The topology derivation method is also effective for

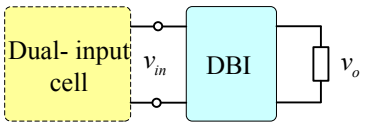

Fig. 2. Structure of the proposed DI-DBI.

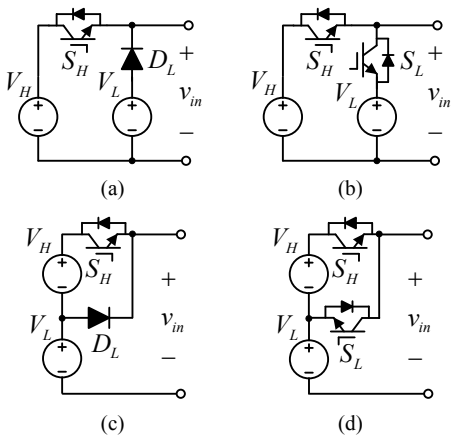

Fig. 3. Topologies of dual-DC-input switching cells: (a) Type I; (b) Type II; (c) Type III; (d) Type IV.

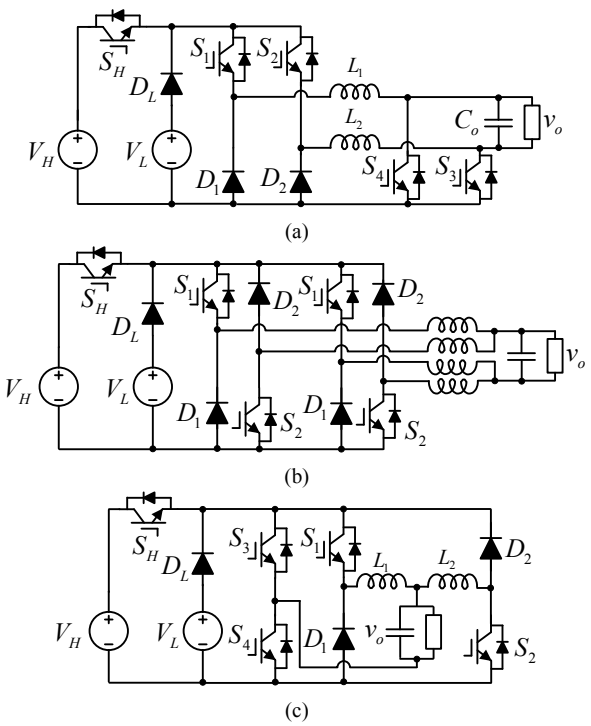

Fig. 4. Topologies of the proposed DI-DBI: (a) Topology I; (b) Topology II; (c) Topology III.

the three dual-input cells shown in Fig. 3(b)-(d). In addition, the single-input DBI used to construct a DI-DBI can be another.

In practical applications, the low voltage DC source V_L can be made up of photovoltaic arrays, fuel cells, batteries, low-voltage DC buses or other low-voltage DC sources. The high voltage DC source V_H can be the output of a Boost converter, whose input is a low voltage DC source V_L. When the low voltage source V_L fully meets the needs of the output voltage v_o, all of the output power can be provided by V_L. When the low voltage source V_L cannot meet the requirements of the output voltage v_o, the output power is provided by V_L and V_H alternatively. Since part of the input power is directly fed to the inverter from V_L, the power losses and power rating of the Boost converter are significantly reduced, which is helpful for the improvement of the overall efficiency.

III. Operation Principle, Modulation Strategy and Characteristics

The operation principles and characteristics of the proposed DI-DBIs are similar to each other. The DI-DBI shown in Fig. 4(a) is taken as an example for analysis to explain the operation principles and characteristics.

A. Operation Principle

As mentioned above, the dual-input switching cell in a DI-DBI is used as the input stage of a traditional dual-buck inverter. However, the DI-DBI is not a simple combination of two circuits. After the dual-input switching cell and a dual-buck inverter are connected as an integrated inverter topology, both the switches in the dual-input switching cell and the switches in the original dual buck inverter can be used to regulate the output voltage/current/power of the AC side. Since the dual-input switching cell is the input stage of the converter, the switch S_H and the diode D_L work regardless of whether the converter operates in the positive half-cycle or negative half-cycle of the AC output voltage. On the other hand, the two buck converters in the original dual-buck inverter operate alternatively in the positive and negative half-cycles of the AC output voltage. More specifically, for the DI-DBI shown in Fig. 4(a), the switch S_3 is kept ON, S_1 and D_1 are operated at a high frequency, while S_2, D_2 and S_4 are kept in the OFF state if the DI-DBI operates in the positive half-cycle of the output voltage v_o. On the other hand, S_1, D_1 and S_3 are always OFF and S_2, D_2 and S_4 are modulated in the negative half-cycle of the output voltage v_o.

Depending on the switching states of these switches, there are a total of six switching states for the DI-DBI shown in Fig. 4(a). The equivalent circuits of these switching states are shown in Fig. 5.

State I [Fig. 5(a)]: The switches S_H, S_1 and S_3 conduct, the other switches and diodes are off. The voltage stress of the diode D_L is clamped by the voltage difference (V_H - V_L). The high voltage source V_H supplies energy to the AC side. The voltage v_{AB} between the mid-points of the two switching legs is clamped by the high side voltage V_H, i.e. v_{AB}=V_H. The output voltage v_o is in its positive half cycle with v_o>0.

State II [Fig. 5(b)]: The switches S_1 and S_3 and the diode D_L are ON, while the other switches and diodes are OFF. The

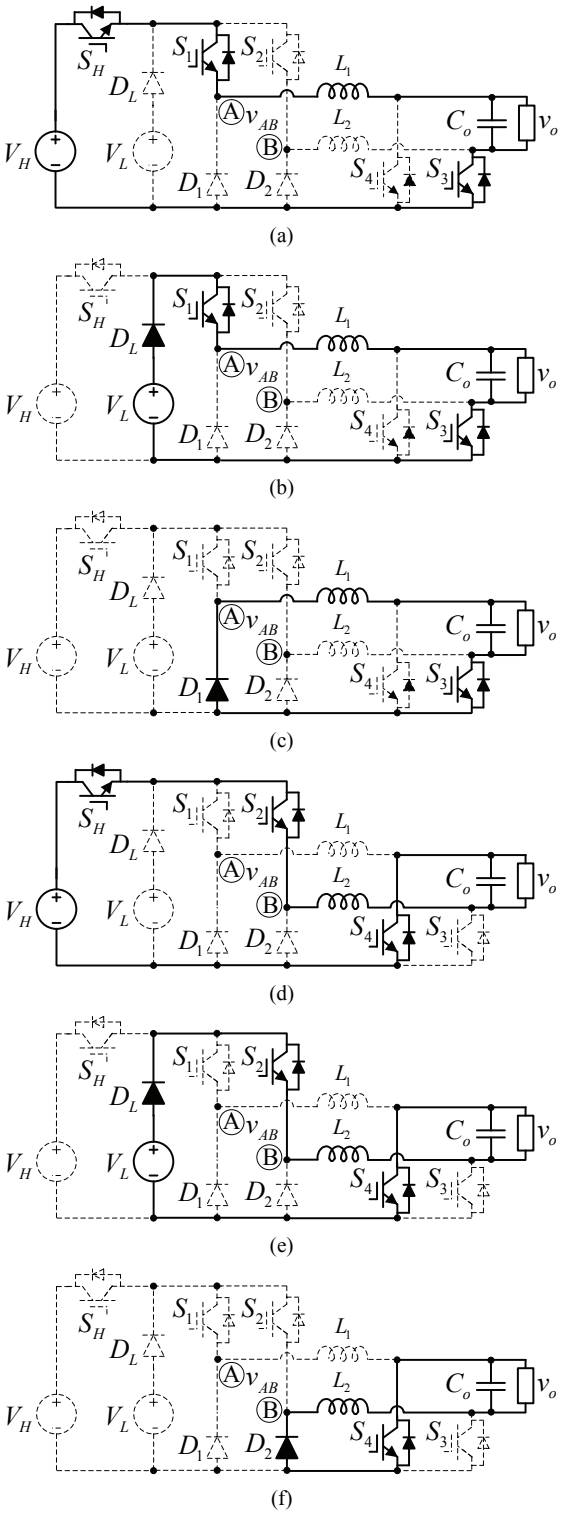

Fig. 5. Equivalent circuits for each of the switching states. (a) v_{AB}=+V_H, v_o>0. (b) v_{AB}=+V_L, v_o>0. (c) v_{AB}=0, v_o>0. (d) v_{AB}=− V_H, v_o<0. (e) v_{AB}=− V_L, v_o<0. (f) v_{AB}=0, v_o<0.

voltage stress of the switch S_H is clamped by voltage difference (V_H - V_L). The low voltage source V_L is used as the input of the dual-buck inverter and supplies energy to the load. v_{AB}=+V_L and v_o>0.

TABLE I
SWITCHING STATES, INPUT SOURCE AND MID-POINTS VOLTAGE

Output voltage	Voltage Source	v_{AB}	S_H	S_1	S_2	S_3	S_4
v_o≥0	V_H	+V_H	1	1	0	1	0
	V_L	+V_L	0	1	0	1	0
	-	0	0	0	0	1	0
v_o≤0	V_H	− V_H	1	0	1	0	1
	V_L	− V_L	0	0	1	0	1
	-	0	0	0	0	0	1

State III [Fig. 5(c)]: The switch S_3 and the diode D_1 are ON, and the other switches and diodes are OFF. The current of the inductor L_1 freewheels through the switch S_3 and the diode D_1. The voltage stress of the switch S_1 is V_L. Neither the high voltage source V_H nor the low voltage source V_L supply energy to the load. v_{AB}=0 and v_o>0.

State IV [Fig. 5(d)]: The switches S_H, S_2 and S_4 are ON, while the other switches and diodes are OFF. The voltage stress of the diode D_L is clamped by the voltage difference (V_H - V_L). The high voltage source V_H supplies energy to the load. v_{AB}= - V_H and v_o<0.

State V [Fig. 5(e)]: The switches S_2 and S_4 and the diode D_L are ON, and the other switches and diodes are OFF. The voltage stress of the switch S_H is clamped by the voltage difference (V_H - V_L). The low voltage source V_L supplies energy to the load. v_{AB}= - V_L and v_o<0.

State VI [Fig. 5(f)]: The switch S_4 and the diode D_2 are ON, while the other switches and diodes are OFF. The current of the inductor L_2 freewheels through the switch S_4 and the diode D_2. The voltage stress of the switch S_1 is V_L. Neither the high voltage source V_H nor the low voltage source V_L supply energy to the load. v_{AB}=0 and v_o<0.

According to the six switching states, the relationship of the switching state, the energy source and the mid-points voltage v_{AB} can be summarized and listed in Table I, where 1 and 0 show when the corresponding switch is in the ON and OFF state, respectively.

From Table I, it can be seen that five voltage levels, i.e. +V_H, +V_L, 0, - V_L and - V_H, are derived from the mid-points of the switching bridge. When the mid-points voltage v_{AB} is +V_H or - V_H, the high voltage source V_H supplies energy to the load. When the mid-points voltage v_{AB} is +V_L or - V_L, the low voltage source V_L supplies energy to the load. Neither V_H nor V_L supply energy to the load when v_{AB} is 0. The switches S_3 and S_4 conduct in the positive and negative half-cycles of the output voltage v_o, respectively. As a result, the two switches work at a low frequency. With the proper control method, the mid-points voltage v_{AB} is able to switch between two adjacent voltage levels, so that there is only one switch working at a high-frequency at any given time.

B. Modulation Strategy

The above analysis indicates that the low voltage source V_L can directly supply energy to the load. It also shows that five voltage levels can be obtained from the mid-points of the switching bridge. The multi-level characteristic is helpful to reduce the voltage stress of the switches and the volume/loss of the output filter. It should be noted that unlike traditional multi-level inverters, which generate balanced multiple voltage-levels, the five voltage-levels generated by the DI-DBI are asymmetrical. The low voltage level is not fixed and is determined directly by the low-voltage DC source V_L.

In practical applications, the low voltage source V_L of a DI-DBI can be the output of a renewable energy source, a low voltage battery, a DC voltage bus and so on. In other words, the voltage of V_L is directly determined by the DC energy source and can be lower than the peak amplitude of the AC output voltage. However, the high voltage source V_H has to be designed to satisfy the modulation index and the peak voltage of the AC output voltage v_o. The voltage V_H can be generated by the V_L through the front-end Boost converter. In order to reduce the power conversion stages and the power losses of the Boost converter, it is necessary to design a modulation strategy to maximize the input power from the V_L port of the DI-DBI.

Due to the symmetrical configuration of the circuit, the operation of the negative half-cycle is similar to that of the positive half-cycle. Therefore, the positive half-cycle of v_o is taken as an example to explain the modulation strategy and characteristics of the converter. According to the relationship between V_L and the instantaneous value of the output voltage v_o, the inverter has two operation modes in the positive half cycle of v_o. As shown in Fig. 6, the inverter works in mode I when the low voltage source V_L is greater than the instantaneous value of the output voltage v_o. In addition, it can be seen that the DI-DBI works in mode II when the low voltage source V_L is lower than the instantaneous value of the output voltage v_o.

Mode I: $V_L \geq v_o$

In this mode, the low voltage source V_L can fully meet the needs of the output voltage v_o. Therefore, the output power of the inverter can be provided directly from the low voltage source V_L. In this mode, the mid-point voltage v_{AB} only needs to be switched between the low voltage level V_L and zero. In other words, the inverter only needs to switch between state II and state III.

Mode II: $V_L \leq v_o$

In this mode, the low voltage source V_L cannot meet the needs of the output voltage v_o. There are two possible modulation strategies. In the first strategy, all of the output power is provided by the high voltage source V_H. The mid-point voltage v_{AB} is switched between the high voltage level V_H and zero. In other words, the inverter only needs to switch between state I and state III. In the second strategy, the output power is provided by both the high voltage source V_H and the low voltage source V_L. The mid-points voltage v_{AB} is switched between the high voltage level V_H and the low voltage level V_L. In other words, the inverter switches between state I and state II. Obviously, the second modulation strategy increases the input power of the V_L port and reduces the switching loss of the high-frequency switches. Therefore, the second modulation strategy is preferred.

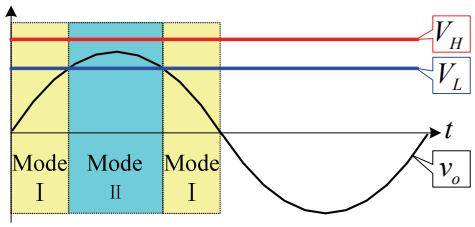

Fig. 6. Operation mode.

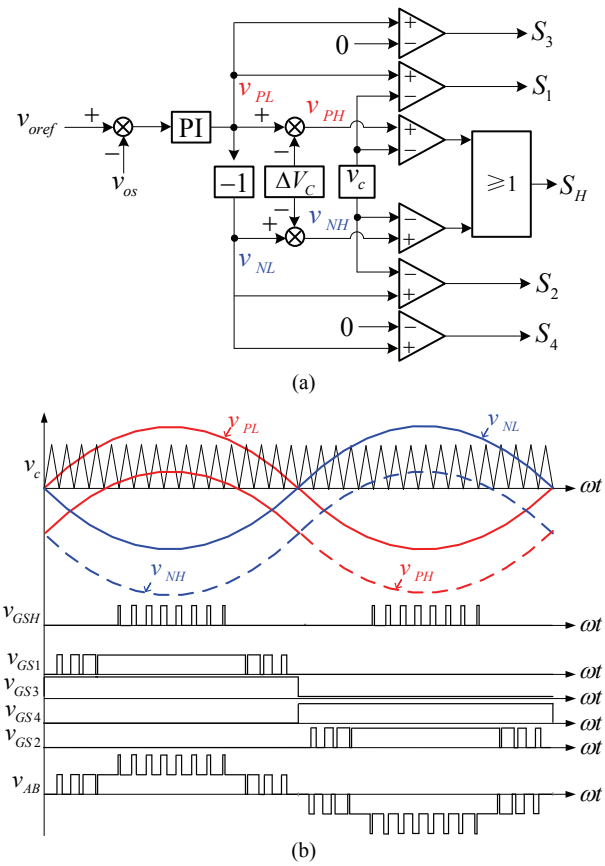

Fig. 7. Modulation strategies: (a) Control block diagram; (b) Key waveforms.

A digital controller is used in this paper. Since there is only one carrier in a digital signal processor, two modulation waves are used to generate the driving signals. The modulation strategies of the DI-DBI are illustrated in Fig. 7, where Fig. 7(a) is a control block diagram for the implementation of the modulation strategy, while Fig. 7(b) shows key waveforms. In Fig. 7, v_{oref} is the reference of the output voltage, v_{os} is the sampled value of the output voltage v_o, v_{PL} is the output of the voltage regulator, v_{NL} is obtained from the reverse of v_{PL}, ΔV_C is the peak-to-peak value of the

carrier v_c, v_{PH} and v_{NH} are obtained by subtracting ΔV_C from v_{NL} and v_{PL}, respectively, v_{gSH} and v_{gS1}~v_{gS4} are the driving signals of the switches S_H and S_1~S_4, respectively, and v_{AB} is the voltage between the mid-points of the two switching bridges.

The driving signals v_{gS1} and v_{gS2} are obtained by comparing v_{PL} and v_{NL} with the carrier v_c. Since the switch S_H is shared by positive and negative Buck converters, the drive signal v_{gSH} is generated by comparing v_{PH} and v_{NH} together with the carrier v_c. In the positive half cycle, when v_{PL} is smaller than ΔV_C, v_{PH} is a negative value and the DI-DBI works in Mode I. In this mode, S_1 switches at a high frequency, while S_H is kept off. When v_{PL} is greater than ΔV_C, v_{PH} is a positive value and the DI-DBI works in Mode II. In this mode, S_H switches at a high frequency, while S_1 is kept on. Like conventional PWM, the peak value of the modulation wave v_{PH} should satisfy the modulation index and be lower than the peak value of the carrier v_c:

$$V_{PH\_peak} \le \Delta V_C \tag{1}$$

where V_{PH_peak} is the peak value of v_{PH}. Therefore, the relationship between the peak value of v_{PL} and ΔV_C should satisfy:

$$V_{PL\_peak} \le 2 \times \Delta V_C \tag{2}$$

where V_{PL_peak} is the peak value of v_{PL}.

C. Characteristics and Analysis

The energy directly transferred from V_L to the load is called direct transmitted energy. The energy transferred to the load through the V_H port is called indirect energy. The more direct energy, the higher the system efficiency. The relationship between the direct energy and a low voltage V_L will be analyzed. In order to simplify the analysis, it is assumed that the output voltage v_o is in phase with the output current i_o. Due to the symmetrical configuration of the circuit, the following only analyzes the relationship in the positive half cycle.

According the above analysis, when $V_L \ge v_o$, all of the energy of the load is provided by the low voltage source V_L. Therefore, the power supplied by the low voltage source V_L is expressed as:

$$p_L = p_o = v_o i_o = 2P_o \sin^2(\omega t) \tag{3}$$

where p_L is the instantaneous power supplied by the low voltage source V_L, and p_o and P_o are the instantaneous and average values of the output power, respectively.

When $V_L \le v_o$, the energy of the load is provided by both the high voltage source V_H and the low voltage source V_L. Therefore:

$$p_H + p_L = p_o \tag{4}$$

where p_H and p_L are the average power provided by the high voltage source V_H and the low voltage source V_L in every switching period. Therefore, p_H and p_L can be expressed as:

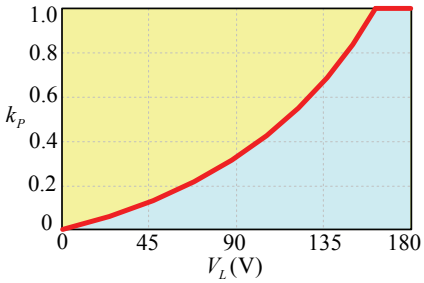

Fig. 8. Direct power transfer ratio.

$$\begin{aligned} p_H &= V_H i_o d_{SH} \\ p_L &= V_L i_o (1 - d_{SH}) \end{aligned} \tag{5}$$

where d_{SH} is the duty cycle of the switch S_H. In addition, according to the volt-second balance of the filter inductor L_1, the duty cycle d_{SH} can be obtained as:

$$d_{SH} = \frac{v_o - V_L}{V_H - V_L} \tag{6}$$

Substituting equation (6) into (4) and (5) yields:

$$p_L = \frac{V_L[V_H - v_o]}{v_o(V_H - V_L)} p_o \tag{7}$$

For better understanding, the direct power ratio k_P of the average power provided by the low voltage source V_L relative to the total output power in every period of the output voltage is calculated as follows:

$$k_P = \frac{\int_0^{\pi} p_L d(\omega t)}{\pi P_o} \tag{8}$$

The curves of the direct power ratio k_P are illustrated in Fig. 8 with the conditions of $v_o = 115\sqrt{2}\sin\omega t$ V and V_H =180V. It can be seen that k_P increase with an increase of V_L. This indicates that as V_L increases, the power transmitted directly from V_L to the load increases, which helps improve the efficiency of the system. When V_L is greater than or equal to the peak amplitude of the output voltage, all of the output power is directly provide by V_L without being processed by the Boost converter. That is to say, all of the power is single-stage power conversion.

Therefore, from the point of view of reducing the conversion stages and power losses of the front-end Boost converter, a higher value of V_L is better. However, the value of V_L is determined by the demand of practical applications.

IV. Experimental Results

Based on aeronautical applications, a 1kW prototype was built and tested based for the DI-DBI topology shown in Fig. 4 (a). As mentioned above, the advantage of the DI-DBI is its ability to improve the efficiency of a system by reducing the indirect power and increasing the direct power. To evaluate the

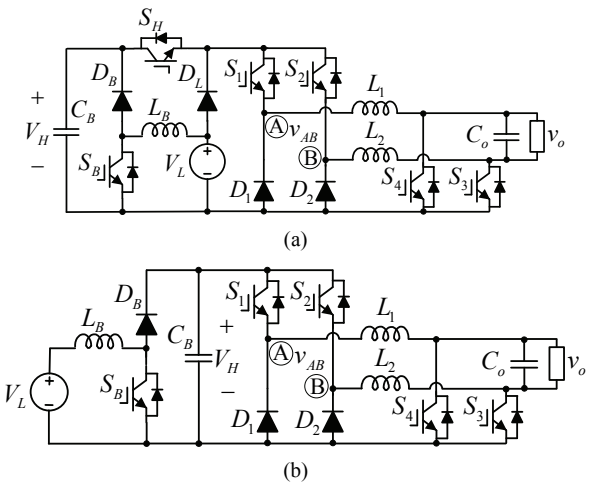

Fig. 9. DC-AC system: (a) DI-DBI-based DC-AC system; (b) DBI-based DC-AC system (v_{AB}=+V_L, v_o>0).

TABLE II
PARAMETERS OF THE PROTOTYPES

Parameter		Value
DI-DBI/DBI	V_H	180V
	V_L	(60-150)V
	v_o	115V/400Hz
	S_H	IPB320N20N3G
	S_1-S_4	IRFB4137PbF
	D_L	SBR20A200CTB
	D_1&D_2	SBR10A300CTB
	L_1&L_2	0.3mH
	C_o	1uF
	Switching frequency	50kHz
Boost	S_B	IXFH69N30P
	D_B	DPG30C300HB
	L_B	320uH
	Switching frequency	100kHz

effectiveness of this method, a traditional prototype of the DBI has also been built. A Boost converter is used as the front-end DC-DC converter for both the DI-DBI and the DBI. Schematics of the DI-DBI and DBI-based DC-AC systems are shown in Fig. 9. For the DI-DBI-based DC-AC system, the low voltage source V_L and high voltage source is V_H are connected to the input and output port of Boost, respectively. By regulating the Boost, V_H is maintained at about 180V. For the DBI-based DC-AC system, the DBI is cascaded with the Boost directly. V_L is connected to the input port of the Boost while V_H is the DC bus voltage between Boost and DBI. It should be noted that the parameters, devices and PCB boards of the two DC-AC systems are exactly the same expect for the DI cell. The parameters and devices are listed in Table II.

A. Experimental Waveforms and Analysis

Fig. 10 shows experimental waveforms of v_{gSH}, v_{gS1}, v_{gS3} and v_o of the DI-DBI with V_L= 60V. The positive and negative

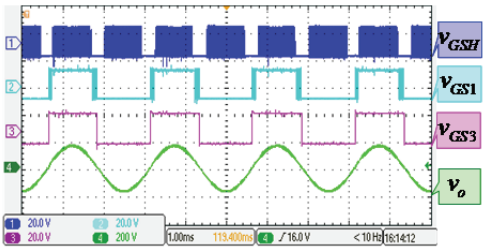

Fig. 10. Waveforms of driving and output voltages with V_L=60V.

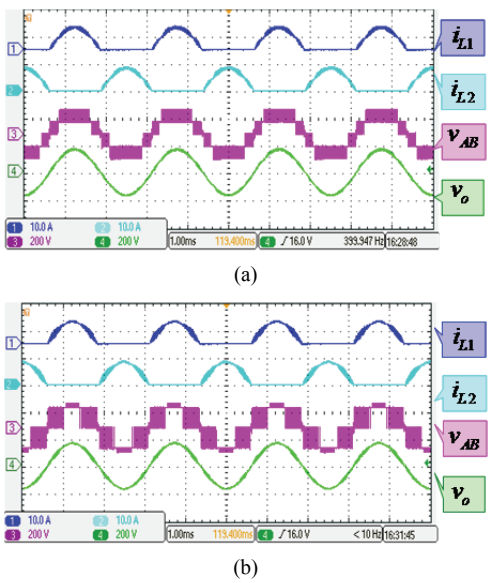

Fig. 11. Waveforms of inductor currents, mid-point and output voltages, (a) V_L=90V, (b) V_L=150V.

voltages of the driving signals are +15V and -9V, respectively. In the positive half cycle of v_o, the switch S_3 remains conductive, while the switches s_H and s_1 are alternately operated at a high frequency. When the switch s_H is operated at a high frequency, the switch s_1 remains on. When the switch s_1 is operated at a high frequency, the switch s_H remains off. In the negative half cycle of v_o, the switches s_1 and s_3 are kept off while the switch s_H is still operated at a high frequency. In the positive half cycle of v_o, when the switch s_H is in high frequency operation, V_L≤v_o. Meanwhile, when the switch s_1 is in high frequency operation, V_L≥v_o. Obviously, when V_L = 60V, because the voltage of V_L is relatively low, the high frequency working time of the switch s_1 is relatively short and the high frequency working time of the switch s_H is relatively long. The experimental waveforms are consistent with the theoretical analysis. Fig. 11(a) and Fig. 11 (b) show the waveforms of i_{L1}, i_{L2}, v_{AB} and v_o with V_L = 90V and V_L = 150V, respectively, where i_{L1} and i_{L2} represent the current through the inductors L_1 and L_2, respectively. It can be seen that the inductors L_1 and L_2 operate in the positive and negative half cycles of v_o, respectively. Five voltage levels are obtained from the mid-points of the switching bridge. Unlike the usual five-level characters, the low voltage level V_L is variable. When V_L = 90V, the five levels are symmetrical while

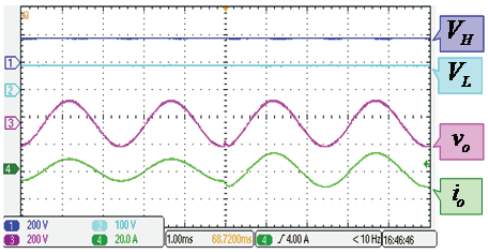

(a)

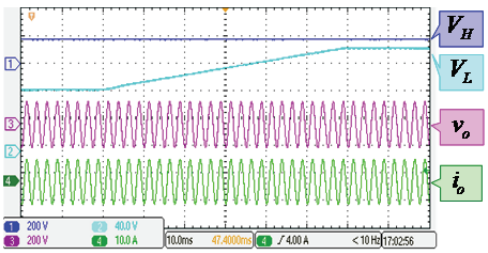

(b)

Fig. 12. Dynamic waveforms, (a) Load step-up, (b) V_L increases voltages.

they are asymmetrical when V_L = 150V. In addition, it can be seen form Fig. 11(b) that the high frequency working time of the switch s_1 is relatively long since the voltage of V_L is relatively high.

Fig. 12(a) shows dynamic waveforms of the DI-DBI with a load step-up when the output voltage of v_o is regulated. It can be seen that the output voltage can be well controlled. Fig. 12(b) shows dynamic waveforms of the DI-DBI with V_L increases when the output voltage of v_o is regulated. It can also be seen that the output voltage can be well controlled.

B. Comparative Analysis

To help the design tradeoff and topology selection, a comparison between DC-AC systems based on the proposed DI-DBI and the traditional DBI-based is necessary.

The efficiency and THD are tested by a power analyzer WT1806 of YOKOGAWA. Fig. 13 shows a wiring diagram for the efficiency and THD tests, where I_B and U_B are the input current and voltage of the Boost converter, I_L and V_L are the input current and voltage of the V_L port of the DI-DBI, I_H and V_H are output current and voltage of the Boost converter, and I_o and V_o are output current and voltage of the DI-DBI, respectively. In the tests, the efficiencies of the Boost, the DI-DBI and the entire DC-AC system are defined as follows:

$$\begin{aligned}\eta_{BOOST} &= \frac{V_H I_H}{V_B I_B}\times 100\% \\ \eta_{DIDBI} &= \frac{V_o I_o}{V_L I_L + V_H I_H}\times 100\% \\ \eta_{\text{DC-AC}} &= \frac{V_o I_o}{V_B I_B + V_L I_L}\times 100\%\end{aligned} \tag{9}$$

Efficiency comparison results between the proposed DI-DBI and the traditional DBI are shown in Fig. 14, where

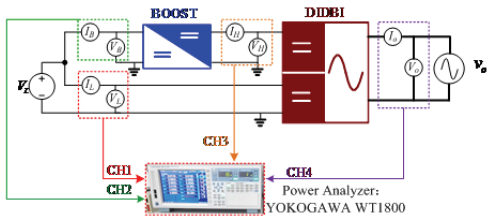

Fig. 13. Wiring diagram for efficiency and THD tests.

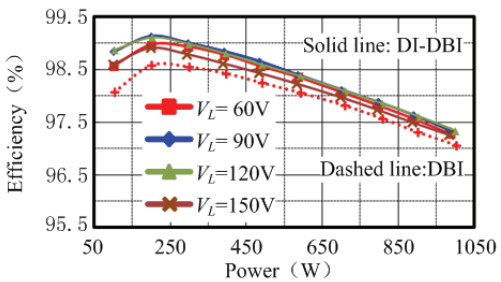

(a)

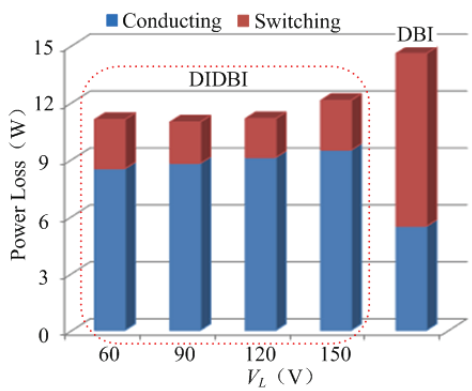

(b)

Fig. 14. Efficiency comparison between the proposed DI-DBI and the traditional DBI: (a) Tested results; (b) Calculated power loss distribution.

Fig. 14(a) shows the tested efficiency and Fig. 14(b) shows the calculated power loss distribution of the DI-DBI. It can be seen in Fig. 14(a) that the efficiency of the DI-DBI is higher than that of the DBI. In addition, the value of V_L has little impact on efficiency. It can be seen in Fig. 14(b) that although more conductive losses are caused by the addition of S_H and D_L, the switching loss of the proposed DI-DBI is reduced significantly thanks to its multilevel characteristics. The total losses of the proposed DI-DBI are lower than those of the traditional DBI, which shows good agreement with the tested results.

Fig. 15 shows an efficiency comparison between DI-DBI-based and traditional DBI-based DC-AC systems, where Fig. 15(a) and Fig. 15(b) show the DC-AC system's tested efficiency results, and Fig. 15(c) shows the calculated power loss distribution between the front-end Boost and the down-stream inverter. It can be seen from Fig. 15(a) and Fig. 15(b) that the efficiency improvement of the proposed DI-DBI-based DC-AC system increases with an increase of

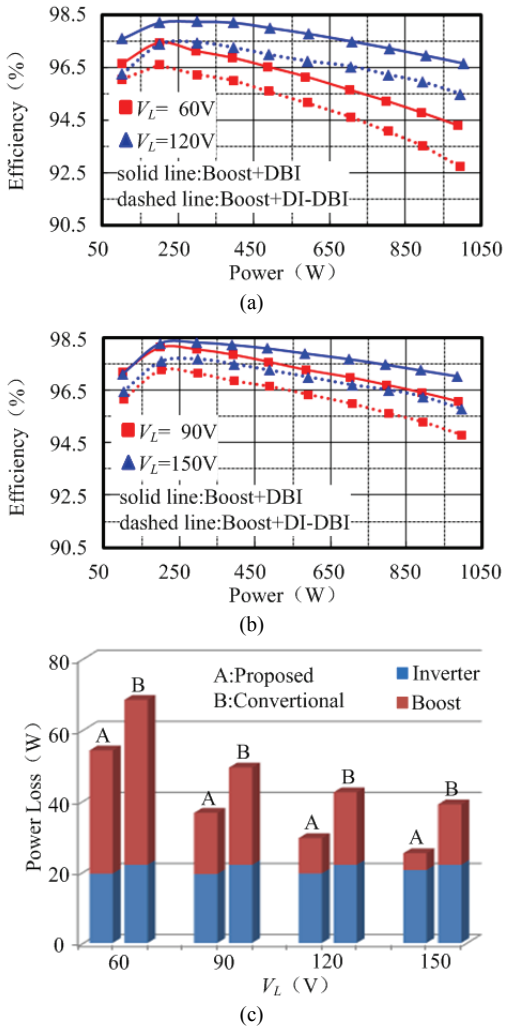

Fig. 15. Efficiency comparison between DI-DBI-based and traditional DBI-based DC-AC systems: (a) Tested results with V_L=60V and V_L=120V; (b) Tested results with V_L=90V and V_L=150V; (c) Power loss distribution.

V_L, and that the efficiency is improved by 1.2% to 1.8%. It can be seen from Fig. 15(c) that the power loss of the frond-end Boost in the DI-DBI-based DC-AC system is smaller than that of the traditional DBI-based DC-AC system and that this advantage becomes more obvious when V_L increases. This is because the power and loss of the frond-end Boost in the proposed system are greatly reduced. Together with the efficiency improvement of the inverter, the efficiency improvement of the proposed DI-DBI-based DC-AC system is more obvious, which coincides with the tested results. The efficiency results verify the effectiveness of the DI-DBI in improving the efficiency of the system.

Thanks to the multi-level characteristics, the harmonics of v_{AB} and can be improved when compared with the traditional DBI. Fig. 16 shows comparison results of the THD of v_{AB}. It can be seen that the THD of v_{AB} in the DI-DBI is much better than that of the DBI in the whole range of V_L. In addition, the calculated and simulated results coincides with the tested

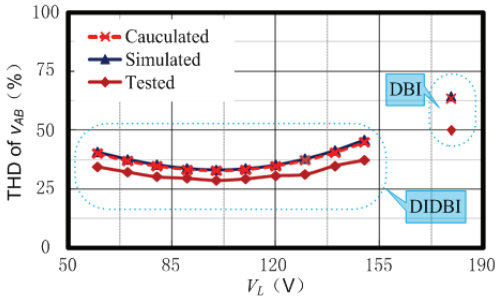

Fig. 16. Comparison of the THD of v_{AB}.

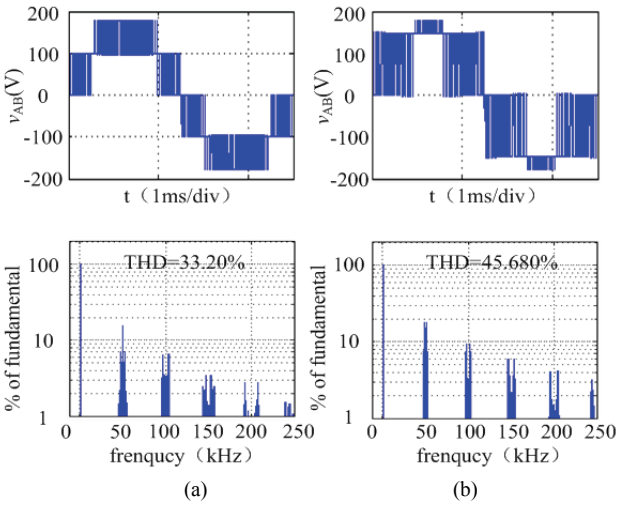

Fig. 17. Harmonic spectrums of v_{AB}: (a) V_L=100V; (b) V_L=150V.

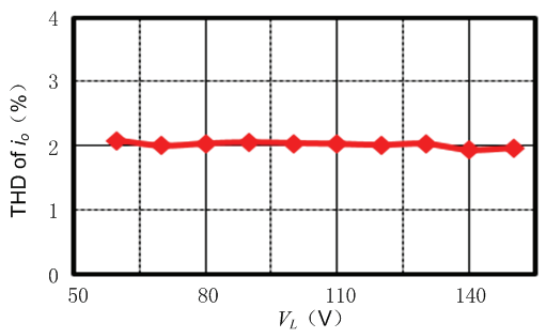

Fig. 18. THD of output current i_o in DI-DBI.

results very well.

The tested results are a little lower than the calculated and simulated results. This is caused by the bandwidth limitation of the power analyzer. Fig. 17 shows the harmonic spectrum analysis of v_{AB} with V_L =100V and V_L =150V. It can be seen that the harmonic spectrum is distributed around the switching frequency and the integer times of the switching frequency. In addition, the harmonic component when V_L =150V is higher than that when V_L =100V. Fig. 18 shows the THD of the output current i_o in the DI-DBI. After filtering, the value of the THD is about 2% in the whole range of V_L, which indicates the effectiveness of the DI-DBI in improving THD.

TABLE III
VOLUME COMPARISON OF THE INDUCTORS FOR THE TWO DC-AC SYSTEMS

			DI-DBI -based	Full-bridge -based
Inverter	Inductor value		0.3mH	0.46mH
	Core	Current through inductor	RMS:6.149A Peak:12.3	RMS:8.696A Peak:12.3
		Type	POCO NPF157026	POCO NPF200026
		Outer Diameter	3.988cm	5.08cm
		Height	1.448cm	1.346cm
	Winding	Number of wingding	90	119
		Outer Diameter	1.75mm	2.1mm
	volume		2*28.87cm^3	42.49cm^3
Boost	Inductor value		0.32mH	0.32mH
	Core	Current through inductor	RMS:13.55 RMS:16.3	RMS:16.667 RMS:19.5
		Type	POCO NPF200026	POCO NPF225026
		Outer Diameter	5.08cm	5.715cm
		Height	1.346cm	1.397cm
	Winding	Number of wingding	100	97
		Outer Diameter	2.5mm	3.0mm
	volume		45.77cm^3	61.96cm^3
Total			103.51 cm^3	104.45cm^3

Fig. 19. Picture of the inductors in DI-DBI-based and full-bridge-based DC-AC systems.

It is well known that the DBI has one more inductor when compared with the traditional full-bridge inverter which seems to be bad for the power density and cost. A volume comparison of the inductor between DI-DBI-based and traditional full-bridge-based DC-AC systems are listed in Table III. Fig. 19 shows a picture of the inductors in the two system, where L_1 and L_2 are the inductors of the DI-DBI, L_{FB} is the inductor of the full-bridge and L_B is the inductor of the Boost. The values of inductors of the two systems are calculated according to the current ripple requirements. Thanks to the multi-level effects, the single inductor value of the DI-DBI is smaller than that of the full-bridge. Secondly, the RMS value of the current though the inductor of the DI-DBI is smaller than that of the full-bridge since the inductor only works in half a cycle. Thirdly, the power of front-end Boost is largely reduced in the DI-DBI-based DC-AC system. As a result, the current through the inductor of the front-end Boost in the proposed DC-AC system is smaller than that in the traditional full-bridge-based DC-AC system. Therefore, although one more inductor is used in the proposed DC-AC system, the total volume of the two systems is about the same.

The power density of an inverter is determined by the inductors. In addition, it is also affected a lot by the thermal stress, heat sink, mechanical stress, etc. Since higher efficiency is achieved, the thermal stress is reduced. In addition, a lot of work has been done to reduce the volume and weight of the output filtering inductor [21]-[23] which can be used to further optimize the inductor of the DI-DBI.

V. CONCLUSIONS

A family of dual-DC-input dual-buck inverters (DI-DBIs) has been proposed for efficiency improvements. A low DC-input port is introduced to a traditional DBI by employing a dual-input switching cell as the input of the DBI. As a result, a low voltage source, whose voltage is lower than the peak amplitude of the AC output voltage, can be directly connected to the DBI to supply power to the AC side in single-stage power conversion. The advantages of high efficiency and high reliability of a traditional DBI can be achieved with the proposed DI-DBIs. In addition, theoretical analysis and experimental verifications indicate that the proposed DI-DBIs have a number of advantages. 1) The conversion stages of a DI-DBI-based DC-AC power system are reduced, since part of the DC input power can be directly fed to the AC side within a single power conversion stage. 2) The power rating and power losses of the front-end Boost converter are reduced. 3) Multi-level characteristics are achieved with the DI-DBIs, which can help to reduce the switching losses and the volume of the output filter. All these features make the proposed DI-DBIs good candidates for high-efficiency and high-reliability DC-AC power systems.

ACKNOWLEDGMENT

This work is supported by National Natural Science Foundation of China (51677085), the Fok Ying-Tong Education Foundation of China, Six talent peaks project in Jiangsu Province (2016-XNYQC-008) and the Fundamental Research Funds for the Central Universities (NO. NE2018 102).

REFERENCES

[1] M. R. Miveh, M. F. Rahmat, A. A. Ghadimi, and M. W. Mustafa, "Power quality improvement in autonomous microgrids using multi-functional voltage source inverters: a comprehensive review," *J. Power Electron.*, Vol. 15, No. 4, pp. 1054-1065, Jul. 2015.

[2] J.-H. Lee, J.-S. Lee, and K.-B. Lee, "Current sensorless MPPT control method for dual-mode PV module-type interleaved flyback inverters," *J. Power Electron.*, Vol. 15, No. 1, pp. 54-64, Jan. 2015.

[3] W. Li, Y. Gu, H. Luo, W. Cui, X. He, and C. Xia, "Topology review and derivation methodology of single-phase transformerless photovoltaic inverters for leakage current suppression," *IEEE Trans. Ind. Electron.*, Vol. 62, No. 7, pp. 4537-4551, Jul. 2015.

[4] D. Barater, E. Lorenzani, C. Concari, G. Franceschini, and G. Buticchi, "Recent advances in single-phase transformerless photovoltaic inverters," *IET Renew. Power Gener.*, Vol. 10, No. 2, pp. 260-273, Feb. 2016.

[5] A. Datta, A. Guha, and G. narayanan, "An advanced gate driver for insulated gate bipolar transistors to eliminate dead-time induced distortions in inverter output," in *IEEE PEDES*, pp. 1-6, 2014.

[6] M. Islam and S. Mekhilef, "Efficient transformerless MOSFET inverter for a grid-tied photovoltaic system," *IEEE Trans. Power Electron.*, Vol. 31, No. 9, pp. 6305-6316, Sep. 2016.

[7] S. V. Araujo, P. Zacharias, and R. Mallwitz, "Highly efficient single-phase transformerless inverters for grid-connected photovoltaic systems," *IEEE Trans. Ind. Electron.*, Vol. 57, No. 9, pp. 3118-3128, Sep. 2010.

[8] D. Garabandic, "Method and apparatus for reducing switching losses in a switching circuit," *U.S. Patent 6847 196*, Aug. 28, 2002.

[9] F. Hong, R. Shan, H. Wang, and Y. Yan, "A novel dual buck full bridge three-level inverte," *Proceedings of the CSEE*, Vol. 28, No. 12, pp. 55-59, Apr. 2008.

[10] R. Chen, J.-S. Zhang, and W. Liu, "Modified dual-buck inverter based on resonant link," *J. Power Electron.*, Vol. 15, No. 6, pp. 1421-1428, Nov. 2015.

[11] F. Hong, J. Liu, B. Ji, Y. Zhou, J. Wang, and C. Wang, "Single inductor dual buck full-bridge inverter," *IEEE Trans. Ind. Electron.*, Vol. 62, No. 8, pp. 4869-4877, Aug. 2015.

[12] L. Zhou and F. Gao, "Dual buck inverter with series connected diodes and single inductor," in *IEEE APEC*, pp. 2259-2263, 2016.

[13] B. Gu, J. Dominic, J.-S. Lai, C.-L. Chen, T. LaBella, and B. F. Chen, "High reliability and efficiency single-phase transformerless inverter for grid-connected photovoltaic systems," *IEEE Trans. Power Electron*., Vol. 28, No. 5, pp. 2235-2245, May 2013.

[14] Z. Yao and L. Xiao, "Two-switch dual-buck grid-connected inverter with hysteresis current control," *IEE Trans. Power Electron.*, Vol. 27, No. 7, pp. 3310-3318, Jul. 2012.

[15] B. Chen, B. Gu, L. Zhang, Z. U. Zahid, J.-S. Lai, Z. Liao, and R. Hao, "A high-efficiency MOSFET transformerless inverter for nonisolated microinverter applications," *IEEE Trans. Power Electron.*, Vol. 30, No. 7, pp. 3610-3622, Jul. 2015.

[16] B. Ji, F. Hong, J. Wang, and S. Huang, "A dual buck three-level PV grid-connected inverter," *J. Power Electron.*, Vol. 15, No. 4, pp. 910-919, Jul. 2015.

[17] L. ZHang, X. Yang, W. Chen, and X. Yao, "An isolated soft-switching bidirectional buck-boost inverter for fuel cell applications," *J. Power Electron.*, Vol. 10, No. 3 pp. 235-244, May 2010.

[18] A. Abramovitz, B. Zhao, and K. M. Smedley, "High-gain single-stage boosting inverter for photovoltaic applications," *IEEE Trans. Power Electron.*, Vol. 31, No. 5, pp. 3550-3558, May 2016.

[19] W. WU, J. Ji, and F. Blaabjerg, "Aalborg inverter - A new type of "Buck in Buck, Boost in Boost" grid-tied inverter," *IEEE Trans. Power Electron.*, Vol. 30, No. 9, pp. 4784-4793, Sep. 2015.

[20] Z. Zhao, M. Xu, Q. Chen, J. S. Lai, and Y. Cho, "Derivation, analysis, and implementation of a Boost-Buck converter-based high-efficiency PV inverter," *IEEE Trans. Power Electron.*, Vol. 27, No. 3, pp. 1304-1313, Mar. 2012.

[21] A. A. Khan and H. Cha, "Dual-Buck Structured High-Reliability and High-Efficiency Single-Stage Buck-Boost Inverters," *IEEE Trans. Ind. Electron.*, Vol. 65, No. 4, pp. 3176-3187, Sept. 2018.

[22] M. Liu, F. Hong, and C. Wang, "Three-level dual buck inverter with coupled-inductance," in *Asia-Pacific Power and Energy Engineering Conference*, pp. 1-4, *2010*.

[23] F. Hong, J. Liu, and B. Ji, "Single inductor dual buck full-bridge inverter," *IEEE Trans. Ind. Electron.*, Vol. 62, No. 8, pp. 4869-4877, Feb. 2015.

Fan Yang was born in Shanxi Province, China, in 1985. She received her B.S. degree in Electrical Engineering from Nanjing Normal University, Nanjing, China, in 2007; and her M.S. degree in Electrical Engineering from the Nanjing University of Aeronautics and Astronautics (NUAA), Nanjing, China, in 2013, where she is presently working towards her Ph.D. degree in Electrical Engineering and Power Drives. Her current research interests include the topologies and control of DC-DC and DC-AC converters.

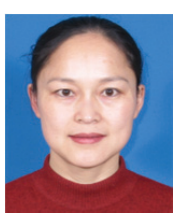

Hongjuan Ge was born in Jiangsu Province, China, in 1966. She received her B.S. and M.S degrees in Engineering from Southeast University, Nanjing, China, in 1985 and 1988, respectively. She received her Ph.D. degree in Electrical Engineering from the Nanjing University of Aeronautics and Astronautics (NUAA), Nanjing, China, in 2007. She joined the Faculty of Electrical Engineering, NUAA, in 1988, where she is presently working as a Professor in the Department of Electrical Engineering, College of Automation Engineering. Her current research interests include the topologies and control for AC-AC matrix converters, and PMSM drives and control. She has authored more than 30 technical papers published in journals and conference proceedings.

Jingfan Yang was born in Jiangsu Province, China, in 1993. She received her B.S. degree in Electrical Engineering from the Nanjing University of Aeronautics and Astronautics (NUAA), Nanjing, China, in 2015, where she is presently working towards her M.S. degree in Electrical Engineering. Her current research interests include the topologies and control of DC-AC converters.

Runyun Dang was born in Gansu Province, China, in 1992. She received her B.S. degree in Electrical Engineering from Nanjing Normal University, Nanjing, China, in 2014. She is presently working towards her M.S. degree in Electrical Engineering at the Nanjing University of Aeronautics and Astronautics (NUAA), Nanjing, China. Her current research interests include the topologies and control of DC-AC converters.

Hongfei Wu (S'11, M'13) was born in Hebei Province, China, in 1985. He received his B.S. and Ph.D. degrees in Electrical Engineering, Power Electronics and Power Drives from the Nanjing University of Aeronautics and Astronautics (NUAA), Nanjing, China, in 2008 and 2013, respectively. From June 2012 to July 2012, he was a guest Ph.D. student at the Institute of Energy Technology, Aalborg University, Aalborg, Denmark. Since 2013, he has been with the Faculty of Electrical Engineering at NUAA, where he is presently working as an Associate Professor in the College of Automation Engineering. He has authored or co-authored more than 100 peer-reviewed papers published in journals and conference proceedings. He is the holder of more than 20 patents. His current research interests include power converters and distributed power generation systems. Dr. Wu was the recipient of an Outstanding Reviewer Award of the *IEEE Transactions on Power Electronics* (2013). He was a recipient of a Changkong Scholar Award of NUAA, in 2017.